SCIENCE CHINA
Technological Sciences

July 2013 Vol.56 No.7: 1723–1732
doi: 10.1007/s11431-013-5243-0

Crack location identification of rotating rotor systems using operating deflection shape data

ZHANG ChunLin, LI Bing*, YANG ZhiBo, XIAO WenRong & HE ZhengJia

State Key Laboratory for Manufacturing Systems Engineering, Xi'an Jiaotong University, Xi'an 710049, China

Received January 21, 2013; accepted March 21, 2013; published online May 7, 2013

Crack location identification, as one key destination of structural health monitoring, is still a challenge for operating rotor systems. The operating deflection shape (ODS), which represents a visual description of the structural vibration patterns under operating conditions, has been gaining importance for structure damage detection in recent years. The ODS carries damage information of a structure, however, it is also difficult to detect weak cracks of rotor directly. The approximate waveform capacity dimension (AWCD) method was successfully applied to damage detection of plates and beam-like structures. In this paper, a strategic approach that combines ODS and weighted AWCD is proposed for crack location identification of the rotating rotor. To eliminate the false peaks of AWCD and obtain desirable results, a weight factor and ODS curvature data are introduced to the expression of the weighted AWCD. The effectiveness of the proposed method is validated by numerical simulation and experimental investigation in a cracked rotor system. The results indicate that the proposed approach not only provides good identifying performance for incipient rotor cracks, but also effectively eliminates the fault peaks introduced by the inflexion locations of ODSs. Moreover, the proposed approach proves promising in detecting crack locations of rotating rotor systems.

cracked rotor, crack location identification, operating deflection shape (ODS), weighted approximate waveform capacity dimension (weighted AWCD)

Citation: Zhang C L, Li B, Yang Z B, et al. Crack location identification of rotating rotor systems using operating deflection shape data. Sci China Tech Sci, 2013, 56: 1723–1732, doi: 10.1007/s11431-013-5243-0

1 Introduction

Fatigue cracks are a potential source of catastrophic failures in rotor systems. Hence, the cracked rotor monitoring has been the focus of interest of many studies in recent decades [1–3]. Crack monitoring for an uninterrupted operating rotor includes three stages: crack detection [4], location identification [5] and quantifiable damage estimation. Many researchers have studied the dynamics [6, 7] and fault diagnosis [8] of a cracked shaft. The work on the crack detection has been mainly based on the vibration signature extraction. Accordingly, important indicators [9–11] and reasonable signal processing techniques [12, 13] have been found for crack detection of the rotor. Though most studies concentrate on qualitatively detecting the crack, it is still a challenge to predict the crack location.

The model-based crack detection methods have drawn special attention for detecting crack locations [14]. Modal curvatures including the natural frequencies are highly sensitive to damage [15–17]. Li et al. [18] adopted the wavelet finite element method (WFEM) in the modal analysis to detect crack location and size for stationary structures. For an operating rotor system, the mode shapes cannot be easily obtained in most practical conditions, and one promising technique is the utility of the operating deflection shape (ODS) which only depends on experimental data from damaged structures [19]. ODSs are vibration response-

*Corresponding author (email: bli@mail.xjtu.edu.cn)

based shapes which are similar to but different from the mode shapes [20]. Sekhar and Babu et al. [21, 22] proposed a generalized ODS as the deflection shape of a structure at any operating speed or subjected to any excitation including multiple loadings. The presence of a crack on the shaft changes the local stiffness and yields a singular point of vibration responses at the crack location along the shaft. Changes in the ODS shape or curvature of the structure like a rotor system will indicate the damage location.

Aiming at the problem that the singular location corresponding to the crack in the ODS cannot be easily seen with naked eyes, especially when a weak crack appears, some signal processing techniques like fractal dimension (FD) and complexity [23] work well in crack detection of rotating rotor when combining with the ODS. FD is considered as a relative measure of the number of basic building blocks that form a pattern [24]. Hadjileontiadis and Douka et al. [25, 26] used FD for damage detection of beams and plates. Fan and Qiao [27] proposed a novel waveform fractal dimension-based damage identification algorithm termed 'approximate waveform capacity dimension (AWCD)'. Whereas considering the higher mode shapes, the false peaks introduced by the inflexion locations may cover up the peaks induced by damage. To overcome this shortcoming, Qiao and Cao [28] verified a specific bijective linear mapping to the original signal before AWCD. These methods have been validated by simulation and experiments for crack identification of beam-like structures [29]. For the rotating rotor system, a strategic approach that combines the ODS and a weighted AWCD was proposed for crack identification in this paper. With a weighting factor and ODS curvature data introduced to the expression of the weighted AWCD, this approach performs well in rotor cracks identification as well as in fault peaks elimination corresponding to the inflexion locations.

The practicability of applying ODS and the weighted AWCD method to identify cracks of rotor system is validated via numerical simulation and experiments in this paper. The rest of the paper is organized as follows. In Section 2, the ODS and the finite element modeling of rotor system with breathing transverse crack on the shaft are presented. Section 3 gives a specific description of the weighted AWCD. At last, the simulation and experimental results are shown in Sections 4 and 5, respectively.

2 A brief review of cracked rotor modeling and operating deflection shape (ODS)

2.1 Finite element modeling of cracked rotor

Much literature has been published concerning the modeling and the breathing mechanism of the cracked rotor [30–32]. Here a brief depiction about the finite element modeling of cracked rotor adopted in this paper is described.

As shown in Figure 1, the rotor shaft is divided into a number of Bernoulli-Euler beam finite elements having four degrees of freedom at each node (shown in Figure 2), where c and k represent the damp and stiffness of the supporting bearings, respectively.

The dynamics equation of the rotor system with a transverse breathing crack, in the inertial coordinate system, can be defined as [10]

$$\boldsymbol{M}\ddot{x}+\left(\boldsymbol{C}+\omega\boldsymbol{G}\right)\dot{x}+\left(\boldsymbol{K}-f\left(t\right)\boldsymbol{K}_{\mathrm{c}}\right)x=\boldsymbol{Q}+\boldsymbol{W}, \tag{1}$$

where $\boldsymbol{M}$, $\boldsymbol{C}$, $\boldsymbol{G}$, adn $\boldsymbol{K}$ mean the mass, damping, gyroscopic and stiffness matrices, $\ddot{\boldsymbol{x}}, \dot{\boldsymbol{x}}$, and $\boldsymbol{x}$ are the acceleration, velocity, and displacement vectors of the cracked rotor system, respectively. ω is the rotating speed of the rotor. The excitation force matrixes $\boldsymbol{Q}$ and $\boldsymbol{W}$ define the vectors of gravity force and unbalance force due to the disc supported on the shaft having mass m and eccentricity e.

In the dynamics equation, the transverse breathing crack effect has been considered in item $f\left(t\right)\boldsymbol{K}_{\mathrm{c}}$. $\boldsymbol{K}_{\mathrm{c}}$ is the additional stiffness matrix due to the transverse crack and the function $f\left(t\right)$ describes the alternating opening and closing process of the breathing crack. Among various crack modeling functions [33, 34], the cosine function modeling is simple and widely used in crack modeling. According to ref. [10], the cosine function modeling $f\left(t\right)$ can be defined as

$$f\left(t\right)=\frac{1}{2}\left(1-\cos\left(\omega t\right)\right). \tag{2}$$

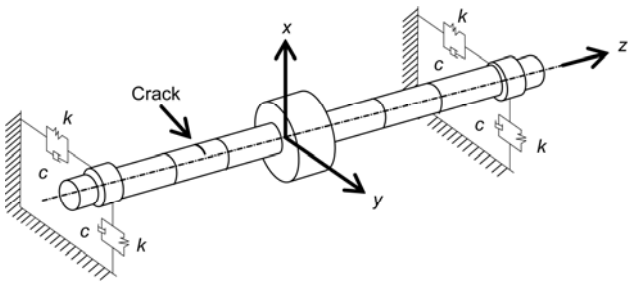

Figure 1 Finite element model of the cracked rotor.

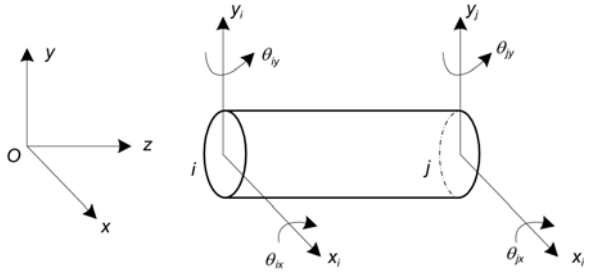

Figure 2 Degrees of freedom of rotor element.

2.2 Operating deflection shape (ODS)

An ODS is defined as the actual displacement or velocity patterns of a structure vibrating at a specific frequency or speed [35, 36]. Then it is further to be depicted more generally as the deflection shape of a structure at any operating speed or subjected to any excitation including multiple loadings [21]. A typical ODS for Jeffcott rotor is shown in Figure 3. The ODS provides a visual description of the vibration patterns of the structure under the operating conditions and anomalies can be detected in terms of geometric features of the structure [37].

ODSs and mode shapes are quite different from one another in a number of ways [38]. The ODS depends on the amplitude and location of loading acting on the structure, while the external excitations do not affect the mode shapes. Yet, ODSs and mode shapes are related to one another. One major connection dwells in that the ODS is the actual structural response from all mode shapes combined and damping included. When the structure is excited at a resonance frequency and the damping is small, the ODS will be similar to the mode shape corresponding to the resonance frequency.

When a structure suffers a crack, the singularity will be introduced in the stiffness and mode shapes of the structure at the location of the crack [39]. The ODS shares the properties of the material, structural and fixing style, and the operating conditions, so changes in ODS shape or curvature of the structure like a rotor system will locate the damage [40]. Simultaneously, the ODS is generally a linear combination of mode shapes, which makes it a more sensitive and feasible approach than mode shape based methods in damage detection [41]. In practice, the ODS is also facile to be observed via experiments.

The ODS defined above describes the actual response of a structure at a particular time, so it is a function of time *t* and the ODS observed at different times may be variational [42]. Practically, this definition also requires a very strict simultaneity of the observation at all the measuring points. In this paper, a generalized definition of the ODS is adopted as the mean envelop amplitude of the responses at each measuring node along the rotating shaft. The mean envelop amplitude is defined as the mean value of a set of amplitude samples on the envelop curve of the vibration response at each node. With this definition, the ODS not only reserves the singularity introduced by the crack but also eliminates the requirement of the simultaneity in the measuring progress. In addition, through the mean operator in calculating the ODS value, the noise and measuring error could be well inhibited.

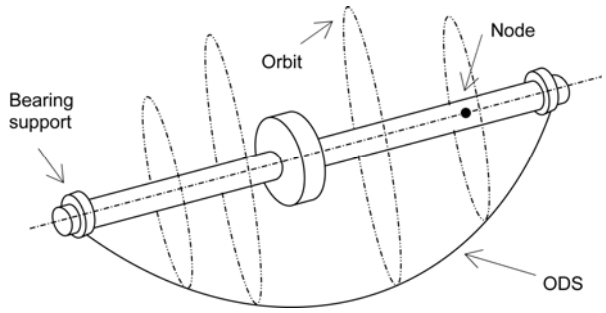

Figure 3 A typical ODS of Jeffcott rotor.

3 Damage identification algorithm

3.1 Introduction of fractal dimension (FD) method

The crack located on a structure, which reduces the local stiffness, is a factor that shifts the vibration signal towards a more complex behavior. The FD is deemed as a measure of the signal complexity in the vibration domain, providing a valuable computational tool to track the existence of a crack [43, 44].

To overcome the probable misleading caused by the FD method when computing a higher mode shape, a novel waveform fractal dimension method, called the approximate waveform capacity dimension (AWCD), was proposed by Qiao and Cao [28] for damage identification. In ref. [28], they derived the formulation of AWCD as

$$\begin{aligned}\mathrm{AWCD} &= \lim_{l\to 0}\frac{\log(L/l)}{\log(1/l)} \approx \frac{\log(L)+\log(N-1)}{\log(N-1)} \\ &= 1+\frac{\log(L)}{\log(N-1)},\end{aligned} \tag{3}$$

where *N* presents the number of steps in the curve; l is the basic mesh of *L*. *L* denotes the total length of the curve, expressed as

$$L=\sum_{i}^{N-1}\mathrm{dist}(P_i,P_{i+1}). \tag{4}$$

By using a sliding window across the operating deflection shape and estimating the AWCD at each position for the regional operating deflection shape inside the window, the peaks on the AWCD indicate the local irregularity of the curve. Unfortunately, these peaks may be introduced not only by the damage on the structure but also by the inflexions of the operating deflection shape, leading to confusion for the damage detection.

Here we illustrate the behaviors of the above methods. Consider the following simulated case

$$f(x)=\begin{cases}\sin(2\pi x)+x^2, & x\in[0,1)\cup(1,2],\\ \sin(2\pi x)+x^2-0.01, & x=1.\end{cases} \tag{5}$$

Figure 4(a) shows the original signal and the zoom figure. In this case, function $f(x)$ has one singular location $x=1$ and four inflexions. Our interest is to identify the singular location that is similar to the crack damage in the structure.

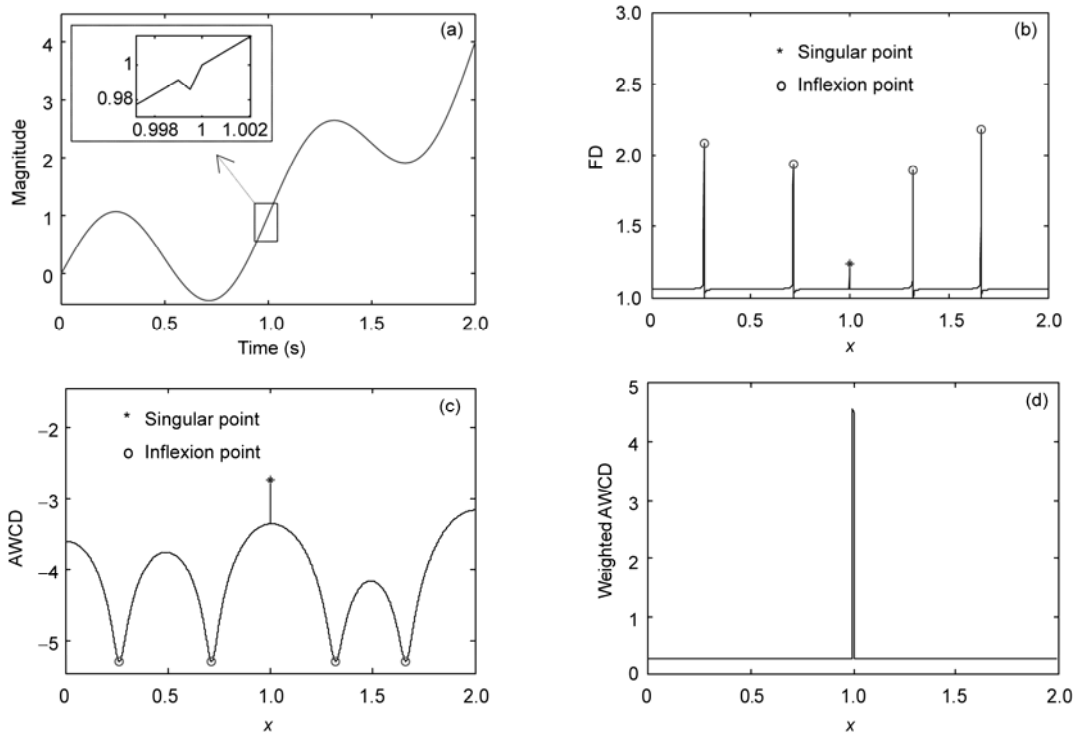

Figure 4 Simulated signal and its transforms. (a) The original signal; (b) the FD values; (c) the AWCD values; (d) the weighted AWCD values.

The signal was processed via FD and AWCD methods, and the results were shown in Figures 4(b) and (c), respectively. Figure 4 shows that FD and AWCD methods are all very sensitive to the singular points and inflexion points due to these two kinds of points share the similarity of increasing the local irregularity of the curve. However, the aliasing of the inflexion locations could not be eliminated for these two methods.

3.2 Damage detection using the weighted approximate waveform capacity dimension (weighted AWCD)

In order to eliminate the false peaks introduced by the inflexion locations which may cover up the peaks induced by damage, Qiao and Cao used a specific bijective linear mapping to the original signal before AWCD. In this article, a weighted AWCD method based on the AWCD approach was developed for the crack location detection.

The weighted AWCD is defined as

$$\mathrm{AWCD}=1+\frac{\log\left(\tilde{L}\right)}{\log\left(N-1\right)}=1+\frac{\log\left(\sum_{i=1}^{N-1}\tilde{L}_i\right)}{\log\left(N-1\right)}, \tag{6}$$

where N is the number of segments on the curvature shape; $\tilde{L}$ denotes the curvature distance of the curve; and the segmental distance $\tilde{L}_i$ is defined as

$$\tilde{L}_i=\sqrt{\left(\tilde{y}_{i+1}-\tilde{y}_i\right)^2+C\left(\tilde{x}_{i+1}-\tilde{x}_i\right)^2}$$

$$=\left(\tilde{x}_{i+1}-\tilde{x}_i\right)\sqrt{\left(\frac{\tilde{y}_{i+1}-\tilde{y}_i}{\tilde{x}_{i+1}-\tilde{x}_i}\right)^2+C}, \tag{7}$$

where C is a weighting factor. The weighted AWCD could separate the singular points from the inflexion points in a curve.

The fundament of the weighted AWCD could be qualitatively explained as follows. As illustrated in Figure 5, when the weighting factor C equals 0, the curvature distance at the singular location is $\tilde{L}_{\mathrm{sin}}$, while the curvature distances at other locations form an assemble $\delta\left(\tilde{L}_{\mathrm{inf}}\right)$. There is usually a far distance $\Delta\tilde{L}$ between $\tilde{L}_{\mathrm{sin}}$ and $\delta\left(\tilde{L}_{\mathrm{inf}}\right)$ due to the essential property that the curvature of an almost smooth curve varies much more sharply at the singular location than at other points including the inflexion location. With the nonlinear logarithm mapping, the global maximum on the weighted AWCD indicates the singular location. The assemble with diameter $\delta\left(\tilde{L}_{\mathrm{inf}}\right)$ induces the oscillation on the weighted AWCD, in which the local extreme points indicate the inflexion locations and make the singular point detection confused, especially when there are two or more singular points. With an appreciate weighting factor $C>0$, $\tilde{L}_{\mathrm{sin}}$ and $\delta\left(\tilde{L}_{\mathrm{inf}}\right)$ are all translated along the axis $\tilde{L}^2$, leading to a very small variation range on the weighted AWCD of $\log\left(\delta\left(\tilde{L}_{\mathrm{inf}}\right)\right)$ and an outstanding $\log\left(\tilde{L}_{\mathrm{sin}}\right)$. Additionally,

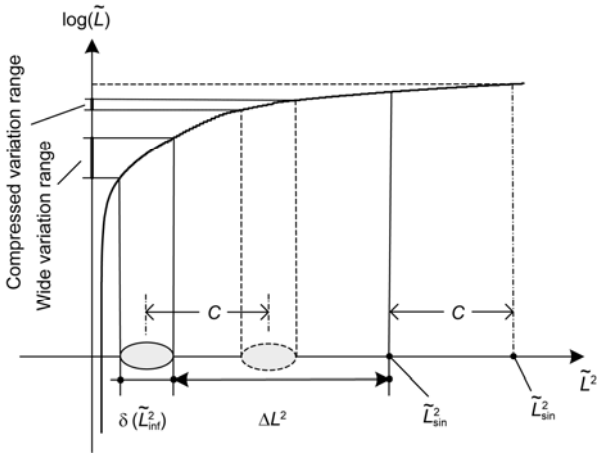

Figure 5 The schematic fundament of weighted AWCD.

formula $\tilde{L}_i$ in eq. (7) contains the second-order difference term of the original curve, which actually expands the distance between $\tilde{L}_{\sin}$ and $\delta\left(\tilde{L}_{\inf}\right)$ and is favorable for separating the singular point from inflexion locations.

In order to detect damage successfully, the weighting factor C has to be chosen carefully. In this article, a strategy for the choice of C is shown as

$$C=\frac{M}{N}\sum_{i=1}^{N-1}\left|\frac{\tilde{y}_{i+1}-\tilde{y}_i}{\tilde{x}_{i+1}-\tilde{x}_i}\right|^2, \tag{8}$$

where N is the number of segments on the curvature shape and M is the number of segments in the sliding window.

The weighted AWCD of the simulated case in eq. (5) was shown in Figure 4(d), where the singular location was clearly detected. In practical crack identification, multi-cracks detection and noise immunity are vital properties. To illustrate how to locate two singular locations using weighted AWCD, let's consider the following simulated case [5].

$$f(x)=\begin{cases}\sin(5.015\pi x)+\sin(7\pi x)+\sin(16\pi x) & 0<x\leqslant 10,\\ \sin(5.007\pi x)+\sin(7\pi x)+\sin(16\pi x) & 10<x\leqslant 20,\\ \sin(4.998\pi x)+\sin(7\pi x)+\sin(16\pi x) & 20<x\leqslant 30.\end{cases} \tag{9}$$

Figure 6(a) shows the original signal and zoom figures. The simulated function $f(x)$ has two singular locations, that is, $x=10$ and $x=20$, while the small changes cannot be clearly seen in the original signal. To simulate noise-contaminated signals, the white Gaussian noise was introduced and the signal-to-noise ratio (SNR) was 40 dB.

To set up an overall assessment on the noise immunity, the Monte Carlo simulation was conducted on 50 pseudo experimental cases. In each simulation case, the polluted signal was analyzed using the weighted AWCD method.

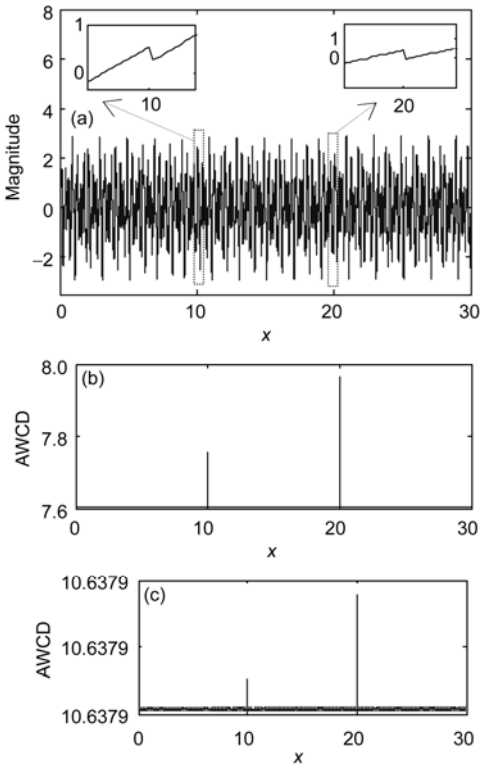

Figure 6 The simulated signal and its weighted AWCD. (a) The original signal and its close-up view; (b) the weighted AWCD curve of the pure signal; (c) the mean weighted AWCD curve of the polluted signal in the Monte Carlo simulations (SNR=40 dB).

Figure 6(b) shows the result of the pure signal, and Figure 6(c) is the average result of the 50 sets of pseudo experiments in the Monte Carlo simulation. Two peaks could be clearly observed on the weighted AWCD curve for both the pure signal and polluted signal and the peaks indicated the singular locations accurately. This simple simulation showed that the weighted AWCD method could detect singular locations reasonably well even when the signal was subjected to certain level of noise.

4 Numerical simulations

Based on the cracked rotor modeling presented in Section 2, the rotor shaft illustrated in Figure 1, having a rigid disc at the center and crack near to it, was divided into 20 elements. The main physical parameters of the rotor system in the numerical simulation were considered as following: shaft length 80 mm, diameter 10 mm, disc mass 4.5 kg, unbalance eccentricity 0.01 mm, initial unbalance phase 0°, bearing supporting stiffness 10^7 N/m, Young modulus 2.1×10^{11} N/m^2, and the density 7850 kg/m^3. The nature frequency of the rotor systems is 26.12 Hz. The location and depth of the transverse crack were considered in the contrastive simulation experiments.

The vibration response at each node along the shaft was

computed for the rotating speed of 1200 r/min. The ODS was then calculated using the mean envelop amplitude of the response at each node. Hence, the weighted AWCD curve was calculated to detect the location of the transverse crack on the shaft. Combining these terms, a flowchart for crack location identification was shown in Figure 7.

The dependence of the weighted AWCD measure on crack depth for a given crack location was investigated firstly. Here, the normalized location $l(l=d/L)$ was considered as a constant for the analysis, where d is the distance between the crack and the first node at the shaft; L is the length of the shaft. The crack location was considered as $l=0.2$ (in the 4th element) and the relative crack depth α (ratio of the crack depth and the shaft diameter) varied from 0.1 to 0.4. The vibration of these weighted AWCD values for the different crack depths including the uncracked case were shown in Figure 8.

For the case of uncracked rotor, only the operating frequency (1X) existed in the frequency response cascade. Because the inflexion location of the ODS could be estimated via the weighted AWCD method, the peak of the weighted AWCD curve indicated the location of the rigid disc due to the residual unbalance. The disc was introduced as a lumped mass and the unbalanced mass would induce new singular boundary at the location of the rigid disc. Fortunately, compared with Figures 8(II)–(V), the weighted AWCD peak at the disc location could be clearly observed only for the rotor without crack or with weak crack. When the relative crack depth reached or forereached 0.2, the weighted AWCD peak at the disc position became unobvious in the weighted AWCD curve.

It can be observed from Figure 8 that the peak values of

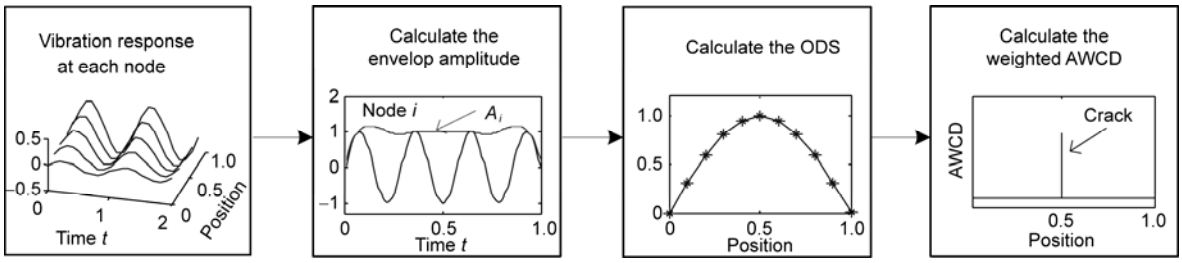

Figure 7 The flowchart for crack location identification using weighted AWCD.

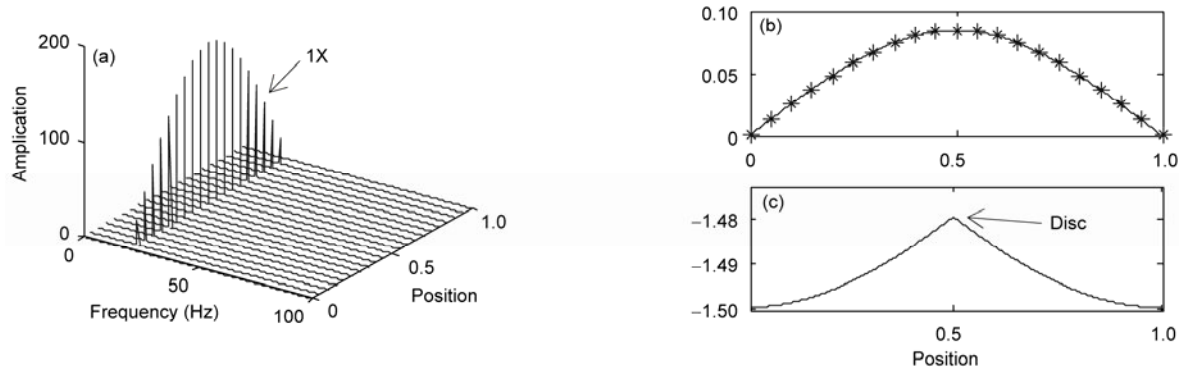

(I) Uncracked rotor.

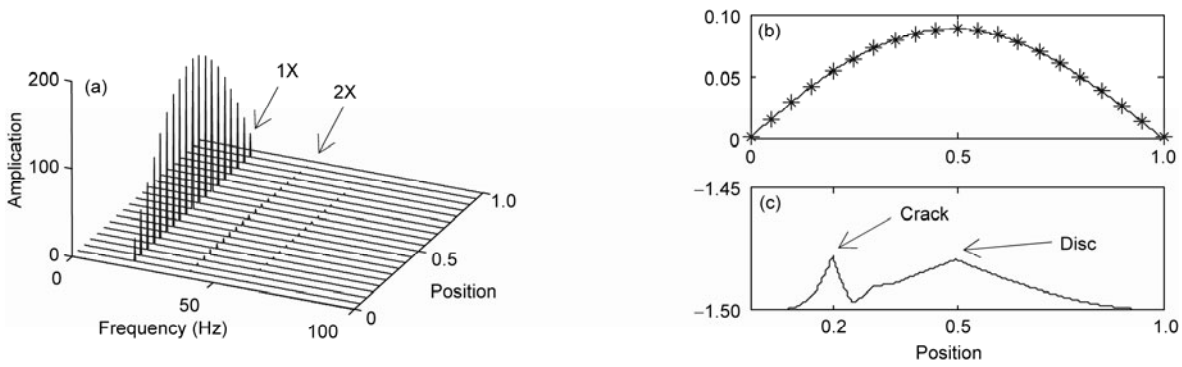

(II) Cracked rotor (α=0.1, l = 0.2).

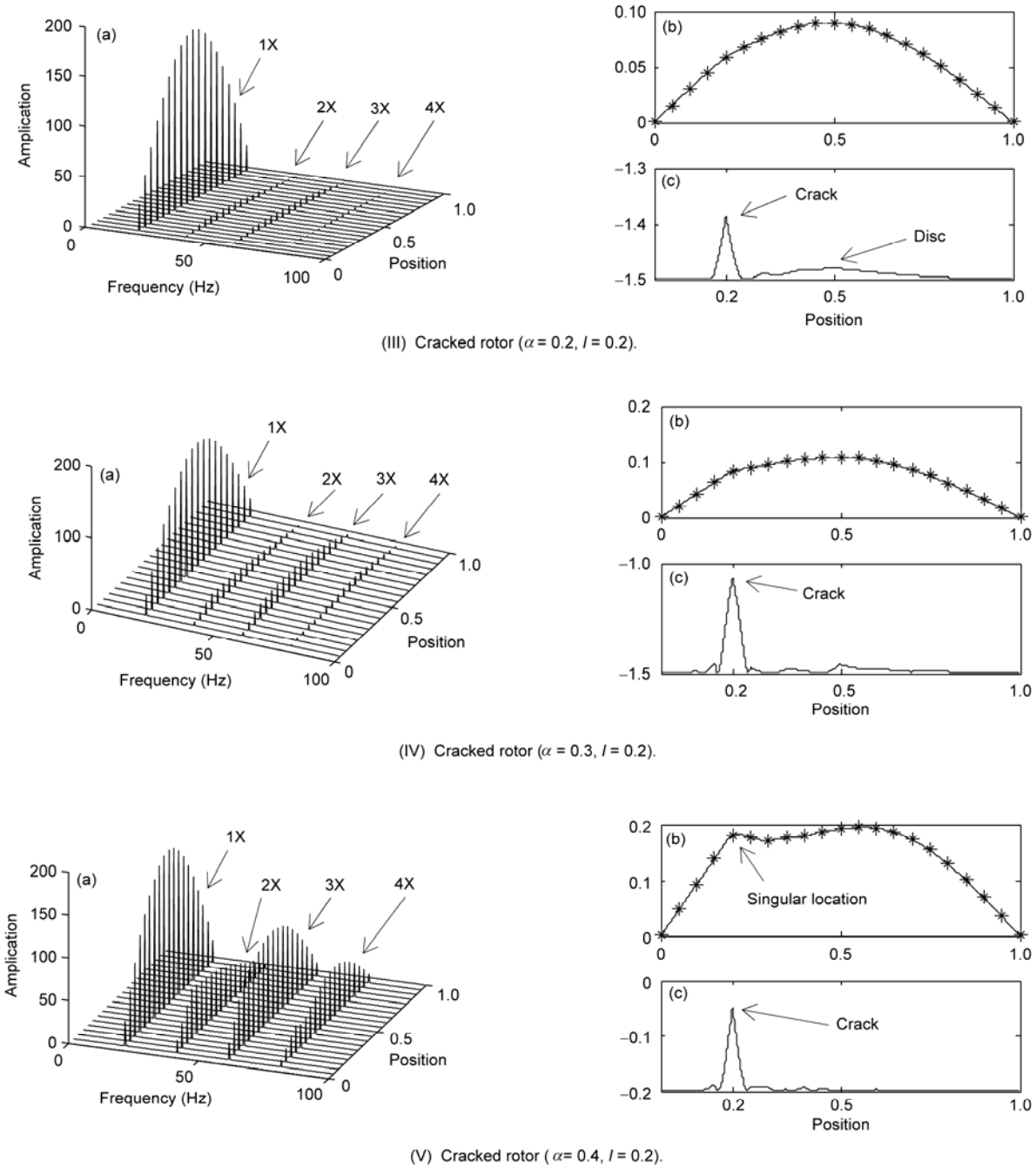

Figure 8 Frequency responses and weighted AWCD curves of cracked rotors with different crack depths. (a) Frequency response cascade; (b) ODS curve; (c) weighted AWCD curve.

the weighted AWCD curve for the cracked shaft appeared at the crack locations. Even for the rotor with weak crack ($\alpha = 0.1$), the peak value at the crack location could be clearly observed and its amplitude seemed larger than that at the disc location. With the prior known disc location in experimental application, the weak crack location could be clearly identified. With the increase of the crack depth, more harmonic components (2X,3X,4X$\cdots$) occurred and their magnitudes became higher. Accordingly, it can be observed from Figure 8 that the peak values of weighted AWCD increased with the increasing crack depth. Thus, the peak value of weighted AWCD along the shaft could identify the crack location, and the increase in its value with time would indicate the crack growth.

In order to show the capability of weighted AWCD to identify different locations of same-depth cracks, for a constant relative crack depth $\alpha = 0.3$, a group of crack cases were constructed according to the crack locations varying

from 0.1 to 0.9 at a spacing of 0.1, excluding the crack case of $l = 0.5$ corresponding to the crack located at the disc position. Figure 9 shows a parallel presentation of the weighted AWCDs associated with these crack cases.

From Figure 9, it can be noted that the crack was identified clearly at the location of the crack with a distinguishable peak value of weighted AWCD at that location. Additionally, the weighted AWCD held an almost steady distinguishable peak along the shaft and the maximum difference of these peaks was less than 0.02. This property allowed weighted AWCD free from the influence caused by damage location.

To show the influence of rotating speed on identification property of weighted AWCD, three cases with the same damage condition ($\alpha = 0.3$, $l = 0.2$) were conducted at different speeds, namely 600, 1800 and 2800 r/min, respectively. It could be observed from Figure 10 that the superior peaks locate the crack position accurately with the speed increase. The results show that the weighted AWCD was not appreciably affected from the speed and enjoyed firm and accurate detection results at different speeds.

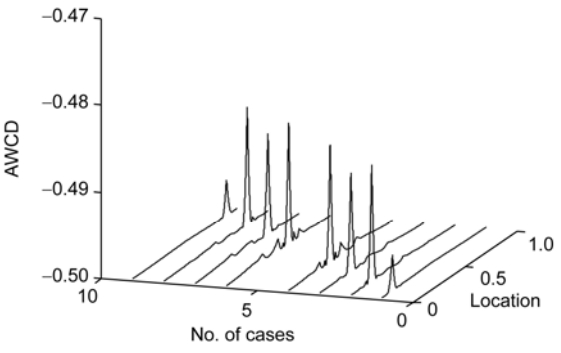

Figure 9 Weighted AWCDs of different crack locations for cracked rotor ($\alpha = 0.3$).

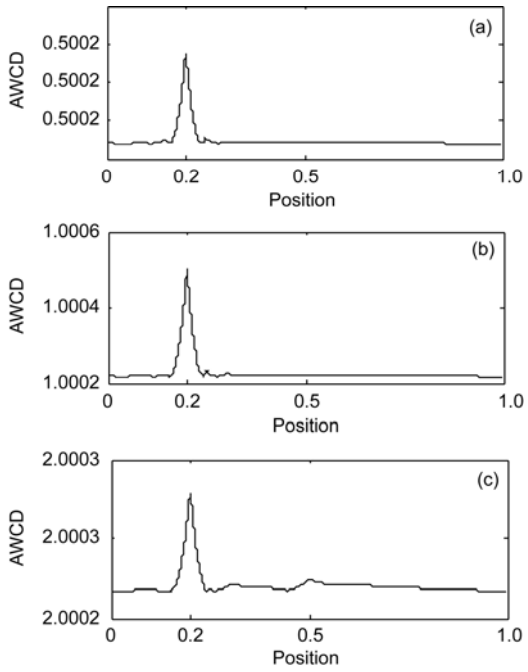

Figure 10 Weighted AWCD of cracked rotor ($\alpha = 0.3$, $l = 0.2$) at different speeds. (a) $w = 600$ r/min; (b) $w = 1800$ r/min; (c) $w = 2800$ r/min.

5 Experimental validations

5.1 Experimental setup

To validate the practicability of the weighted AWCD method to identify cracks of rotor systems, experiments were conducted on the Bently rotor test system in which a shaft was supported on bearing seats with a rigid disc mounted on the shaft. The experimental setup was shown in Figure 11. The geometry of the shaft was shown in Figure 12. The length of the shaft $L_1 = 420$ mm, diameter $D_1 = 10$ mm and natural frequency of the shaft was found experimentally as $f_0 = 35.93$ Hz. The rotating speed of the shaft was 1500 r/min, namely 25 Hz.

The experiments were conducted using a cracked shaft which was divided into 28 elements. The crack on the shaft was generated by wire cutting with the width of less than 0.1 mm. The location and depth of the crack were $e = 145$ mm (at the 10th node) and $a = 2$ mm, respectively. Therefore, the respective normalized crack location and depth were $l_c = 0.345$ and $\alpha = 0.2$.

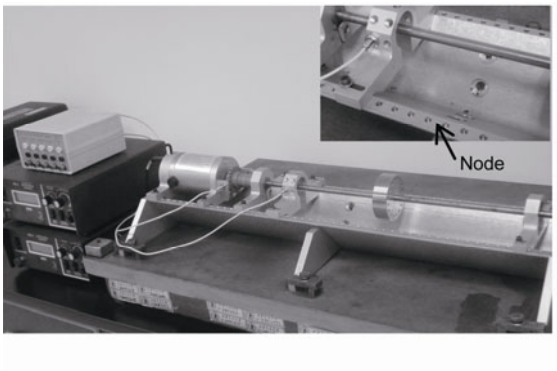

Figure 11 Bently rotor test system.

Figure 12 shows the schematic diagram of the experimental setup. The location and diameter of the disc were $L_2 = 315$ mm and $D_2 = 60$ mm. Therefore, the normalized location of the disc center was $l_d = 0.75$. The eddy current sensor fixed on the seat was adopted for the vibration measurement. By moving the sensor seat along the shaft, the signals at different locations on the shaft were acquired via the SONY-EX which is a computer controlled data acquisition system. In the experimental study, the sampling frequency $f_s = 3200$ Hz and 12800 data points were collected.

5.2 Experimental results

The vibration responses of every node construct the ODS

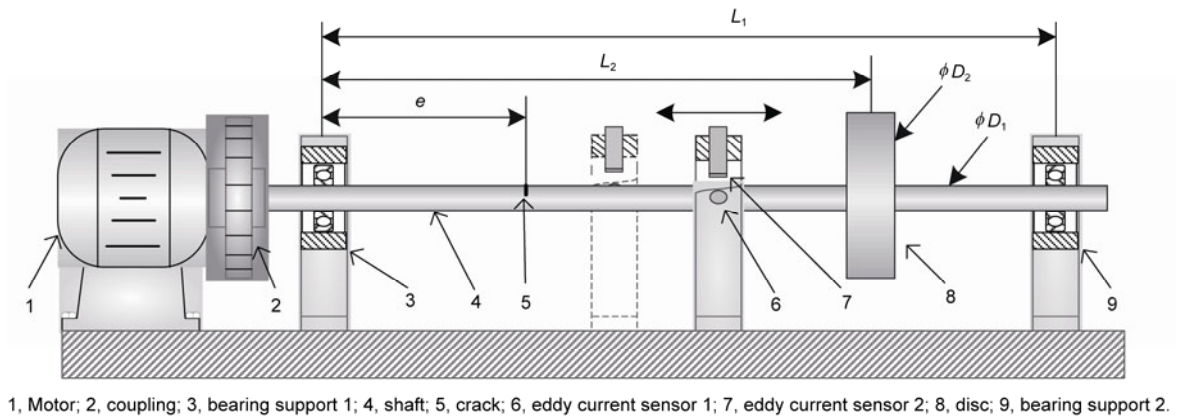

Figure 12 Schematic diagram of the experimental setup.

curve of the cracked rotor. Figure 13 shows the vibration responses at the 29th measuring node of the shaft in both time and frequency domains. The ODS value was calculated using the envelop amplitude of the responses which would eliminate the effect of the measurement noise. Subsequently, the other ODS values at other nodes were calculated with the same procedure.

Figure 14 shows the ODS curve of the cracked rotor and its weighted AWCD curve is shown in Figure 15. The horizontal coordinate represented the normalized location l. The peak point at l_1=0.343 in the weighted AWCD curve well matches the exact crack location of l_c=0.345, and a lower peak l_2=0.73 represented the location of the disc. The discrepance of l_d and l_2 dwelled in the effect of geometric thickness of the disc. Additionally, the peak at the crack location was more shaper than that at the disc location, which was similar to the simulation results.

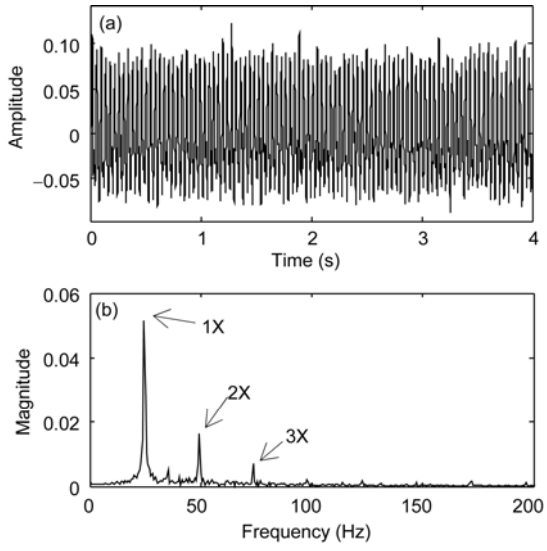

Figure 13 The vibration responses at the 29th node. (a) Vibration signal in time domain; (b) frequency spectrum.

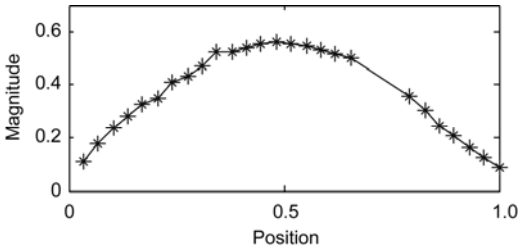

Figure 14 ODS curve of the cracked rotor.

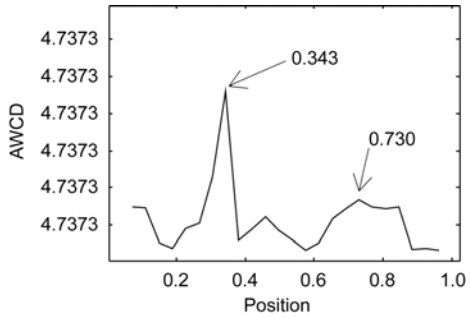

Figure 15 The weighted AWCD curve of the cracked rotor.

6 Conclusion

In this paper, a strategic approach based on ODS measurement data and weighted AWCD was proposed to detect locations of cracks in rotating rotor systems. To address the problem that the singular location corresponding to the crack in the ODS cannot be easily observed with naked eyes, especially when a weak crack appears, a post-processing method named weighted AWCD was presented. The weighted AWCD method could accurately identify the crack locations. In addition, it also performed well in eliminating the fault peaks corresponding to inflexion locations caused by the higher mode shapes. The peaks on the weighted AWCD curve accurately indicated the crack locations. Simulation studies and experiments were conducted

to validate the performance of the proposed approach. The results illustrated that the proposed approach is potentially a good tool in detecting crack locations of rotating rotor systems.

This work was supported by the National Natural Science Foundation of China (Grant No. 51035007), the National Basic Research Program of China ("973" Program) (Grant No. 2011CB706805), and Program for Changjiang Scholars and Innovative Research Team in University.

1 Zbigniew K, Jerzy T S. Controlled deflection approach for rotor crack detection. J Eng Gas Turb Power-T ASME, 2012, 134: 092502
2 Chen J L, Zi Y Y, He Z J, et al. Construction of adaptive redundant multiwavelet packet and its application to compound faults detection of rotating machinery. Sci China Tech Sci, 2012, 55: 2083–2090
3 Han Q K, Chu F L. The effect of transverse crack upon parametric instability of a rotor-bearing system with an asymmetric disk. Int J Nonlinear Sci Numer Sim, 2012, 17: 5189–5200
4 Babu T S, Srikanth S, Sekhar A S. Hilbert-Huang transform for detection and monitoring of crack in a transcient rotor. Mech Syst Signal Process, 2008, 22: 905–914
5 Xiang J W, Matsumoto T, Long J Q, et al. A simple method to detect cracks in beam-like structures. Smart Struct Syst, 2012, 9(4): 335–353
6 Hamidi L, Piand J B, Pastorel H, et al. Modal parameters for cracked rotors: modes and comparisons. J Sound Vib, 1994, 175(2): 265–278
7 Wang S S, Ren Q L. Relationship between local damage and structural dynamic behavior. Sci China Tech Sci, 2012, 55(12): 3257–3262
8 Sekhar A S, Prabhu B S. Condition monitoring of cracked rotors through transient response. Mech Mach Theor, 1998, 33(8): 1167–1175
9 Guo D, Chu F L, He Y Y. Vibration analysis of rotor with transverse surface cracks. ASME Turbo Expo, 2003, GT2003–38041
10 Sinou J J, Lees A W. The influence of cracks in rotating shafts. J Sound Vib, 2005, 285: 1015–1037
11 Patel T H, Darpe A K. Influence of crack breathing model on nonlinear dynamics of a cracked rotor. J Sound Vib, 2008, 311: 953–972
12 Lei Y G, Zuo M J. Fault diagnosis of rotating machinery using an improved HHT based on EEMD and sensitive IMFs. Meas Sci Technol, 2009, 20: 125701
13 Lu W X, Chu F L. Shaft crack identification based on vibration and AE signals. Shock Vibr, 2011, 18: 115–126
14 Yang Z B, Chen X F, Tian S H, et al. Multiple damages detection in beam based approximate waveform capacity dimension. Struct Eng Mech, 2012, 41: 663–673
15 Xiang J W, Liang M. Multiple crack identification using frequency measurement. World Academy of Science, J Eng Technol, 2011, 52: 311–316
16 Wang N F, Zhang X M. Compliant mechanisms design based on pairs of curves. Sci China Tech Sci, 2012, 55: 2099–2106
17 Xiang J W, Matsumoto T, Wang Y X, et al. A hybrid of interval wavelets and wavelet finite element model for damage detection in structures. Cmes-comput Model Eng Sci, 2011, 81(3): 269–294
18 Li B, Chen X F, Ma J X, et al. Detection of crack location and size in structures using wavelet finite element methods. J Sound Vib, 2005, 285: 767–782
19 Myung K Y, Dirk H, John W. Local damage detection with the global fitting method using operating deflection shape data. J Nondestruct Eval, 2010, 29: 25–37
20 Zhu X Q, Law S S. Wavelet-based crack identification of bridge beam from operational deflection time history. Int J Solids Struct, 2006, 43(7-8): 2299–2317
21 Babu T R, Sekhar A S. Detection of two cracks in a rotor-bearing system using amplitude deviation curve. J Sound Vib, 2008, 314: 457–464
22 Saravanan K, Sekhar A S. Crack detecting in a rotor by operational deflection shape and kurtosis using laser vibrometer measurements. J Vib Control, 2012, DOI: 10.1177/1077546312444770
23 Yang D X, Hu N Q, Zhang C Z. Early fault detection of electric machiner rotor-bearing system based on complexity measure analysis. Chin Soc for Elec Eng, 2004, 24(11): 126–129
24 Katz M J. Fractals and the analysis of waveforms. Comput Biol Med, 1988, 18(3): 145–156
25 Hadjileontiadis L J, Douka E, Trochidis A. Fractal dimension analysis for crack identification in beam structures. Mech Syst Signal Process, 2005, 19: 659–674
26 Hadjileontiadis L J, Rekanos I T. Detection of explosive lung and bowel sunds by means of fractal dimension. IEEE Signal Process Lett, 1988, 10: 311–314
27 Fan W, Qiao P Z. Vibration-based damage identification methods: a review and comparative study. Struct Health Monit, 2011, 10(1): 83–111
28 Qiao P Z, Cao M S. Waveform fractal dimension for mode shape-based damage identification of beam-type structures. Int J Solids Struct, 2008, 45: 5946–5961
29 Cao M S, Qiao P Z. Integrated wavelet transform and its application to vibration mode shape data for the damage detection of beam-type structures. Smart Mater Struct, 2008, 17(5): 055014
30 Darpe A K, Chawla A, Gupta K. Analysis of the response of a cracked Jeffcott rotor to axial excitation. J Sound Vib, 2002, 249(3): 429–445
31 Darpe A K, Gupta K, Chawla A. Coupled bending, longitudinal and torsional vibrations of a cracked rotor. J Sound Vib, 2004, 269: 33–60
32 Jun O S, Eun H J, Earmme Y Y, et al. Modelling and vibration analysis of a simple rotor with a breathing crack. J Sound Vib, 1992, 155(2): 273–290
33 Liu J T, Du P A, Zhang Z Y. A general model of fatigue crack growth under variable amplitude loading. Sci China Tech Sci, 2012, 55: 673–683
34 Chu F, Wang F L, Wang X G, et al. A model for parameter estimation of multistage centrifugal compressor and compressor performance analysis using genetic algorithm. Sci China Tech Sci, 2012, 55: 1–13
35 Waldron K, Ghoshal A, Schulz M J, et al. Damage detection using finite element and laser operational deflection shapes. Finite Elem Anal Design, 2002, 38: 193–226
36 Nelson F C. Rotor dynamics without equations. Int J Comadem, 2007, 10(3): 2–10
37 Pai P F, Young L G. Damage detection of beams using operational deflection shapes. Int J Solids Struct, 2001, 38: 3161–3192
38 Richardson M H. Is it a mode shape, or an operating deflection shape? Sound Vib, 1997, 31(1): 54–61
39 Chaudhari T D, Maiti S K. A study of vibration of geometrically segmented beams with and without crack. Int J Solids Struct, 2000, 37: 761–779
40 Xiang J W, Matsumoto T, Long J Q, et al. Identification of damage locations based on operating deflection shape. J Nondestructive Eval, 2012, DOI: 10.1080/10589759.2012.716437
41 Pai P F, Jin S. Locating structural damage by detecting boundary effects. J Sound Vib, 2000, 231(4): 1079–1110
42 Dossing O. Structural stroboscopy-measurement of operational deflection shapes. Sound Vib, 1988: 18–26
43 Hadjileontiadis L J, Douka E. Crack detection in plates using fractal dimension. Eng Struct, 2007, 29: 1612–1625
44 Carlin M. Measuring the complexity of non-fractal shapes by a fractal method. Pattern Recognit Lett, 2000, 21(11): 1013–1017